Translational relevance of behavioral, neural, and electroencephalographic profiles in a mouse model of post-traumatic stress disorder

Kaiwen Xi [a,1], Xin Huang [a,b,1], Tiaotiao Liu [c,1], Yang Liu [a], Honghui Mao [a], Mengmeng Wang [a], Dayun Feng [a,d], Wenting Wang [a], Baolin Guo [a,*], Shengxi Wu [a,**]

[a] Department of Neurobiology, School of Basic Medicine, Fourth Military Medical University, Xi'an, China
[b] Department of Neurology, Xijing Hospital, Fourth Military Medical University, Xi'an, China
[c] School of Biomedical Engineering and Technology, Tianjin Medical University, Tianjin, China
[d] Department of Neurosurgery, Tangdu Hospital, Fourth Military Medical University, Xi'an, China

ARTICLE INFO

ABSTRACT

Post-traumatic stress disorder (PTSD) is a severe, long-term psychological disorder triggered by distressing events. The neural basis and underlying mechanisms of PTSD are not completely understood. Therefore, it is important to determine the pathology of PTSD using reliable animal models that mimic the symptoms of patients. However, the lack of evidence on the clinical relevance of PTSD animal models makes it difficult to interpret preclinical studies from a translational perspective. In this study, we performed a comprehensive screening of the behavioral, neuronal, glial, and electroencephalographic (EEG) profiles in the single prolonged stress and electric foot shock (SPS&S) mouse model. Based on the clinical features of PTSD, we observed fearful and excessive responses to trauma-related environments in the SPS&S mouse model that lasted longer than 14 days. The mice exhibited a defective and strong resistance to the extinction of fear memories caused by auditory cues and also showed enhanced innate fear induced by visual stimuli with concomitant phobias and anxiety. Furthermore, neurons, astrocytes, and microglia in PTSD-related brain regions were activated, supporting abnormal brain activation and neuroimmune changes. EEG assessment also revealed decreased power and impaired coupling strength between cortical regions. These results demonstrated that the SPS&S mouse model recapitulates the behavioral symptoms as well as neural and EEG profiles of PTSD patients, justifying the preclinical use of this mouse model.

1. Introduction

Post-traumatic stress disorder (PTSD) is a severe mental health condition that often occurs following distressing events (Johnson et al., 2021). Over half the global population may experience a natural disaster or other traumatic events in their lifetime with the possibility of triggering PTSD development (Yabuki and Fukunaga 2019). Besides the disaster victims, rescue workers have been shown to exhibit PTSD symptoms (Schlenger et al., 2002). Thus, PTSD is a profound public health issue that affects numerous populations throughout the world. PTSD patients are characterized by an exaggerated response to contextual memory, impairment of fear extinction, and sometimes cognitive and learning deficits (Yehuda 2002). However, treatments for PTSD are limited in clinical practice due to its unknown pathogenesis (Zhou et al., 2021).

Current knowledge of the multifaceted pathogenesis of PTSD relies on preclinical studies performed in a diverse array of rodent models (Johnson et al., 2021), which play a pivotal role in delineating the functions of neural circuits and underlying PTSD molecular mechanisms. However, PTSD is heterogeneous due to the variety of triggering events (Yehuda 2002), and its heterogeneity in humans is a challenge in selecting an appropriate rodent model for preclinical studies. Especially, the development of state-of-the-art research tools relying on transgenic animals, mouse models have gained increasing importance. Currently, there are no systematic evaluations to assess whether mouse models recapitulate all aspects of human PTSD.
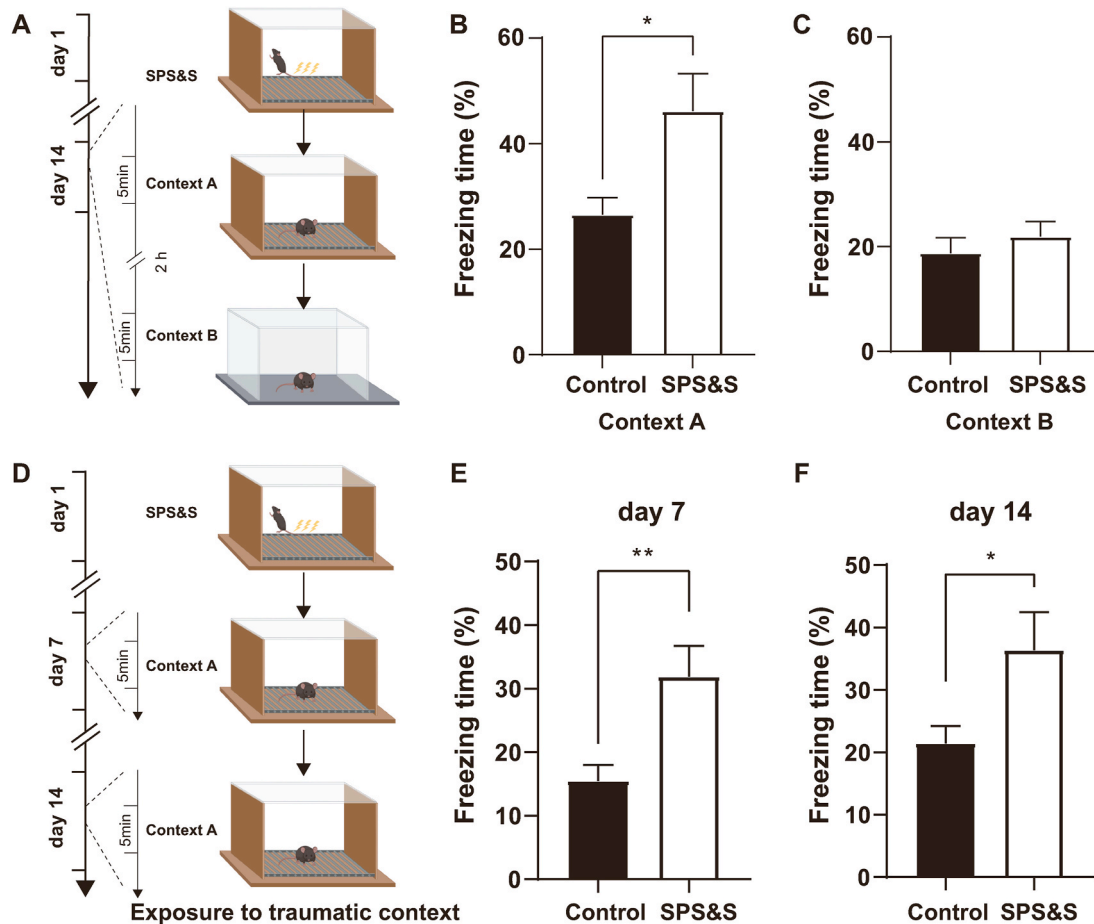
Fig. 1. SPS&S mice show excessive fear responses to traumatic environments. A Diagram of the experimental procedure. B Compared with control mice, SPS&S mice exhibited longer freezing times in Context A (Two-tailed unpaired separate variance estimation *t*-test, t = 2.399, df = 12.41, P = 0.0330, n = 10 per group). C SPS&S mice and control mice exhibited similar freezing times in Context B (Two-tailed unpaired *t*-test, t = 0.7689, df = 18, *P* = 0.4519, n = 10 per group). D Diagram of the experimental procedure. Mice were exposed to Context A, which is related to the traumatic event, on days 7 and 14 after model establishment. E Compared with control mice, SPS&S mice exhibited longer freezing times in Context A on day 7 (Two-tailed unpaired *t*-test, t = 3.008 df = 18, *p* = 0.0076, n = 10 per group). F Compared with control mice, SPS&S mice exhibited longer freezing times in Context A on day 14 (Mann-Whitney *U* test, U = 20, P = 0.0232, *P* < 0.05, n = 10 per group). *P* < 0.05, **P* < 0.01.

Single prolonged stress (SPS) has been widely employed in animals to develop PTSD models. SPS-stressed rats have shown enhanced conditioned fear responses (Imanaka et al., 2006), sensitized fear responses (Iwamoto et al., 2007), exaggerated acoustic startle responses (Khan and Liberzon 2004), and anxiety-like behaviors (Fan et al., 2021) in multiple studies. However, relevant studies in mice are limited. Our previous studies modified the SPS stress protocol by introducing a single inescapable electric foot shock after the SPS procedure (Wang et al., 2008; Feng et al., 2020). This single prolonged stress and electric foot shock (SPS&S) mouse model demonstrated hyperarousal, another core symptom of PTSD, in addition to other core symptoms. However, the fear-related behavioral phenotypes of this model, such as impaired fear extinction, innate fearful behaviors, as well as a phobia to the environment and social communications, have not been fully characterized. Also, patients with PTSD show altered functional magnetic resonance imaging (fMRI) and electroencephalography (EEG) results, which could be used for PTSD diagnosis and evaluation of interventions (Bryant et al., 2021; Schlumpf et al., 2021). Whether PTSD animal models display similar functional readouts is still unclear. Moreover, the excessive immune state is one of the critical alterations in PTSD patients in the peripheral immune system and in the brain (Bhatt et al., 2020). Therefore, testing the alterations of glial cells in certain brain regions would be critical to demonstrate the significance of PTSD mouse models in preclinical neuro-immunological research studies. Thus, a systematic

assessment of PTSD-relevant behavioral phenotypes, screening of changes in specific brain regions, and measurement of EEG profiles in PTSD animal models are significant from a translational perspective. Also, understanding correlations between neurobiology observations and behaviors is critical for employing these animal models in preclinical research.

In this study, we systematically screened PTSD-relevant fearful behaviors, observed alterations in neurons and glia in PTSD-vulnerable brain regions, and monitored EEG changes following PTSD stress in SPS&S mice. We found that SPS&S mice showed typical PTSD-like behavioral abnormalities, including excessive responses to trauma-related contexts, impaired fear extinction, enhanced innate fear, as well as concomitant phobias and anxiety. Besides these behavioral phenotypes, the mouse model also demonstrated neural and glial activation in PTSD-related brain regions, altered EEG power, and impaired coupling relationships between cortical regions. Our findings provide systematic experimental data for SPS&S mouse model phenotypes, including its behavioral, neural, and EEG phenotypes, and demonstrate the translational relevance of the model to bridge the gap between preclinical research and clinical practice.
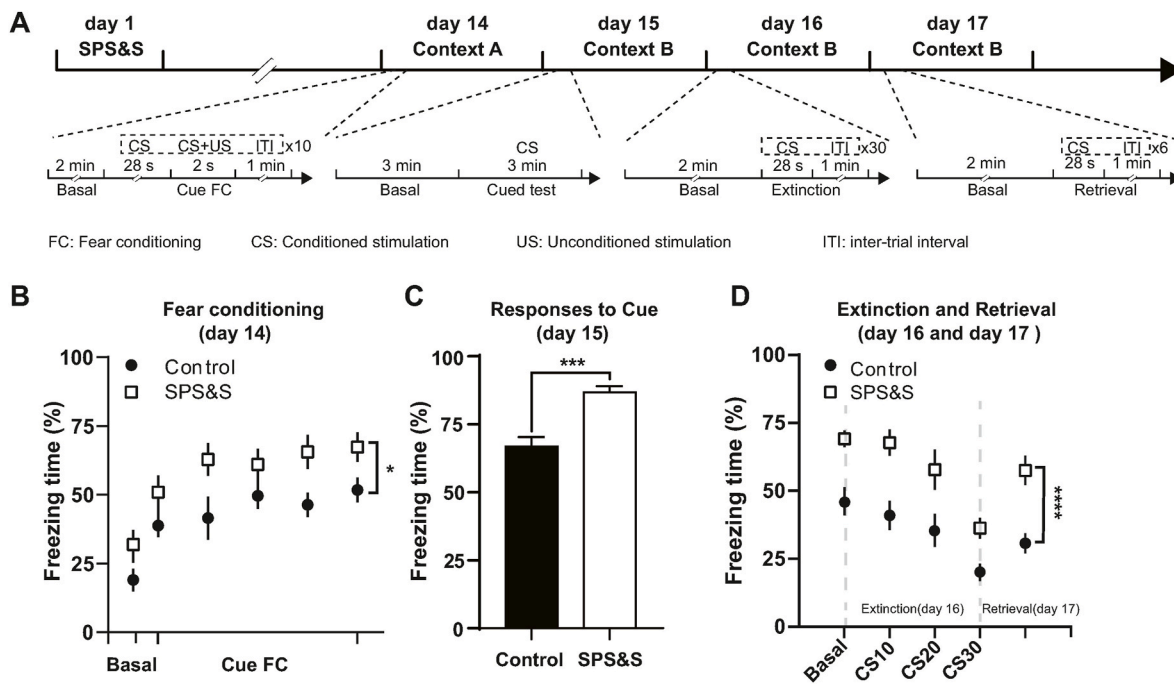
Fig. 2. SPS&S mice show enhanced fear responses to sound cues and impaired fear extinction. A Diagram of the training, extinction, and retrieval procedures. B Freezing times of SPS&S mice and control mice during the fear conditioning training on day 14. SPS&S mice exhibited a longer freezing time baseline and final freezing time after the sound cue stimulation session (Repeated measurement ANOVA, $F_{between\ group}$ = 5.204, df1 = 1, df2 = 18, $P_{between\ group}$ = 0.035; $F_{within\ group}$ = 23.371, df1 = 5, df2 = 90, $P_{within\ group}$ < 0.0001; n = 10 per group). C Compared with control mice, SPS&S mice exhibited longer freezing times in Context B during the sound cue stimulation (Two-tailed unpaired *t*-test, t = 4.067, df = 18, P = 0.0007, n = 10 per group). D Compared with control mice, SPS&S mice exhibited a longer freezing time baseline before and after extinction of fear memory in Context B (Repeated measurement ANOVA, $F_{between\ group}$ = 34.411, df1 = 1, df2 = 18, $P_{between\ group}$ < 0.0001; $F_{within\ group}$ = 27.781, df1 = 1.539, df2 = 27.708, $P_{within\ group}$ < 0.0001, n = 10 per group). *P < 0.05, ****p < 0.0001.

2. Methods

2.1. Animals

All procedures were approved by the Institutional Animal Care and Use Committee of the Fourth Military Medical University (FMMU) and conformed to the Guide for the Care and Use of Laboratory Animals published by the National Institutes of Health (NIH). Mice were housed in a room maintained at a constant temperature and on a 12-h light/dark cycle. Water and food were available *ad libitum*. C57BL/6 male mice aged 2–6 months old were used in the experiments.

2.2. SPS&S stress protocol

The SPS&S stress procedure was performed as previously described (Feng et al., 2020). Briefly, four stressors used in this study were restraint stress, forced swim, deep anesthesia, and unconditioned foot shock. First, we used the mouse fetter to constraint the experimental group of mice for 4 h in their own home cage. Second, the mice were forced to swim in a plastic tub filled with water (25 °C) for 20 min. Next, mice were exposed to an appropriate amount of ether until they were totally anesthetized. Finally, an unconditioned foot shock (0.8 mA, 5 s) was delivered in a context box, Context A, and the mice were subsequently returned to their home cage and left undisturbed. The control group mice were also put in the same context box Context A for 5 s without shock to experience environmental stimuli.

2.3. Fear conditioning and extinction test

We performed a contextual and cued fear test as described in previous reports (Shoji et al., 2014; Feng et al., 2020); the experiments are depicted in Fig. 1 & 2. These tests were conducted simultaneously between 1 h after the onset of the light phase (8:00 a.m. to 6:00 p.m.) and

1 h before the dark phase. The fear conditioning tests used commercial equipment (Vanbi, China). The animals were habituated in the experimental room for at least 2 h with the light on before the tests. Before and after each trial, all devices were cleaned with 75% alcohol and paper towels and air-dried. All animals were returned to their home cage after each trial.

For the contextual fear test, we designed two sets of experiments. To test fear responses to the traumatic environment., SPS&S animals were placed on day 14 in Context A for 300-s exploration. After a 2-h break in their home cage, the animals were placed in a new environment Context B (distinct wall and floor compared to Context A) for another 300-s exploration. For the other set of experiments, we explored the time courses of fear behaviors; on day 7 the mice were placed in the conditioning chamber Context A and were allowed to freely explore the chamber for 300 s. Subsequently, they were returned to their home cage and left undisturbed after the exploration. On day 14, the animals were placed in Context A for 300-s exploration and were then returned to their home cage.

The conditioning and cued fear test protocols were performed, as shown in Fig. 2. Briefly, on day 14 after SPS&S, the animals were placed in Context A, and the fear conditioning training was performed as previously reported (Hartley et al., 2019). Each animal was allowed to explore the chamber freely for 120 s, then an auditory cue, comprising a tone of 75 dB, 4500 Hz was presented for 30 s as a conditioned stimulation (CS) and a foot shock (0.8 mA) performed in the last 2 s of the tone as an unconditioned stimulation (US). This presentation of CS-US pairing was repeated for 10 rounds with 60 s of inter-trial interval (ITI). On day 15, the animals were placed in Context B for the cued test and were allowed to explore the new environment for 3 min following which the same tone (75 dB, 4500 Hz) was introduced for 3 min. On day 16, the extinction test was performed in Context B as previously described (Hartley et al., 2016). The mice were placed in Context B, and a short 120-s baseline was used to test initial freezing as a measure of fear

generalization to the new context. Next, mice were presented with the same CS without US for 30 s, following which a 60-s ITI was presented. This CS-ITI pairing was presented for 30 rounds. On day 17, the retrieval test was performed to recall the extinction. The animals were placed in Context B and the CS paired with a 60-s ITI was conducted for 6 rounds after a short 120-s baseline.

2.4. Odor-evoked innate fear test

We performed the odor-evoked innate fear test as described in a previous report (Xu et al., 2012; Paolini 2014). Briefly, the animals were placed in the experimental environment for 2 h before the experiments. The experiment was performed in a cubic chamber (50cm × 50 cm × 40 cm) and cat litter with 400 μL bobcat urine (LegUp Enterprises, US) and clean cat litter with saline were collected on the morning of the experiment. The experimental site was divided into 25 equal parts and the cat litter with fresh urine and clean cat litter with saline were put on the cubic chamber diagonally. Before the experiment, the cubic chamber was cleaned with 75% alcohol. Each animal was put in the center of the chamber after the chamber was dried and then recorded it for 10 min. Entries into cat litter were measured to investigate the level of odor-invoked innate fear.

2.5. Looming-evoked innate fear test

A shelter (diameter = 8 cm, length = 10 cm) was placed in the home cage of the mice for habituation for 3 d before the tests. The animals were kept in the experimental room for 2 h before the experiments. The looming test equipment was homemade as previously described (Zhou et al., 2019). We placed the animals into a transparent Plexiglas cubic chamber (50cm × 50 cm × 50 cm) with the bedding from their home cage at the bottom. A video encoded to display an expanding black circle was positioned on top of the cubic chamber. We set the stimulus expanded to 50° over 250 ms and the code to repeat the stimulus 10 times with an interval of 1 s. First, we placed the animal in the center of the cubic chamber and habituated it for at least 10 min. After the habituation, when the mouse was exploring the environment in the center of the chamber, we began to display the video. We measured the time from the mice discovering the looming to hiding in the shelter to evaluate the innate fear level evoked by looming.

2.6. Novel object phobia test

We performed the novel object phobia test as previously reported (Chauke et al., 2012). The two groups of mice were kept in the experimental environment for 2 h before the experiments to habituate. The same novel object (2cm × 2 cm × 2 cm, rough surface) was placed in the same location of the home cage and the trajectory of each mouse in the observation area was recorded for 10 min. We measured the bouts, latency of approach, and time of investigation to evaluate the phobia.

2.7. Social phobia test

The social phobia test was carried out as described in a previous report (Lukas et al., 2011). The animals were placed in the experimental room for 2 h before the experiment to habituate. The social phobia test device (Noldus, Netherlands) consisted of a fan-shaped space (10cm × 8cm × 7 cm) in the fenced isolation bar of organic glass and the rest space for mice to explore freely. The device was cleaned before the experiment. An age-matched male mouse unfamiliar to the experimental mice was placed in the isolation bar and the experimental mice were in the middle of the device. The behavior of the experimental mice was recorded for 10 min. After each trial, the device was cleaned with 75% alcohol and air-dried.

2.8. Open field test

The open-field test was performed as described by (Feng et al., 2015) The two groups of mice were placed in the experimental room for 2 h and were allowed to habituate for 3–5 min before the experiment. Subsequently, each mouse was moved from the home cage to the center of the cubic chamber (50 cm × 50 cm × 50 cm) and the behavior was recorded for 10 min. After each trial, the chamber was cleaned to repeat the experiment for the rest of the animals.

### 2.9. Elevated plus-maze test

We performed the elevated plus-maze test as previously reported (Guo et al., 2019). Animals were placed in the experimental room for 2 h and were allowed to habituate for 3–5 min before the experiment. The elevated plus-maze consisted of two black Plexiglas arms, two opposing closed arms, two opposing open arms (50 cm × 10 cm), and a central area (10 cm × 10 cm) made up the maze; the walls of the closed arms were composed of black acrylic. After habituation, the mouse was held in the central area, making the animal face open arms, and the behavior was recorded for 5 min. The maze was cleaned between the experiments for the rest of the animals.

2.10. Immunofluorescence histochemistry

Mice were placed into Context A and explored for 5 min freely. Then we put the mice back to their home cages. Following a 1.5-h break, mice were anesthetized with isoflurane and transcardially perfused with 0.01 M phosphate-buffered saline (PBS), pH 7.4 followed by 4% paraformaldehyde in 0.2 M PBS, pH 7.4. Brains were rapidly removed and fixed using the same fixative for 4 h at 4 °C. After dehydrating twice with 30% sucrose for 48 h at 4 °C, brain sections (50 μm) were sliced on a freezing microtome. The sections from each group (3–6 sections from each region) were rinsed in a blocking solution for 2 h and incubated overnight (4 °C) with primary antibodies: c-Fos (1:1500, CST), glial fibrillary acidic protein (GFAP) (1:250, Gene Tex), ionized calcium-binding adaptor molecule 1 (IBA1) (1:500, WAKO). Sections were then washed with PBS and probed with secondary antibodies: Alexa Fluor 594-conjugated anti-rabbit secondary IgG (Invitrogen) or Alexa Fluor 594-conjugated anti-goat IgG (Invitrogen) for 4 h. All images were captured with a confocal microscope (FV3000, Olympus, Japan), and processed with the Imaris software (v.7.7.1, Bitplane, Switzerland). For cell counting, 3–6 sections per region were counted per animal with the Imaris software by experimenters blinded to the groups.

2.11. EEG recording

We performed EEG surgery on 8- to 12-week-old mice after they were anesthetized with 1%–2% isoflurane. One electrode screw each for intracranial frontal and parietal EEG and a common ground/reference above the cerebellum were implanted with the stereotaxic device. Electrodes were soldered to EEG/EMG headmount (Pinnacle Technology Inc., #8402-SS, USA), and dental acrylic was used to encase the connection. Mice had at least 2 weeks to recover from the EEG surgery. For the postoperative pain management, 1 mg/kg Buprenorphine SR (Every 72 h) and 1 mg/kg Meloxicam (Every 12 h) were subcutaneously injected. Any pain signs of mice were monitored during the recovery week following the surgeries. After the recovery, spontaneous EEG signals were recorded for 4 h in the light cycle. One week after the first round of recording, mice were exposed to the SPS&S procedure and then recovered for 2 weeks in their home cage. After the recovery, spontaneous EEG signals for 4 h were recorded similarly. All signals were digitized at a sampling frequency of 1000 Hz, filtered (1–100 Hz bandpass for EEG), and acquired by using the Sirenia Acquisition program (Pinnacle Technology Inc.). Data collected during wake episodes were analyzed offline by using Matlab (Math Works, R2016a). Before
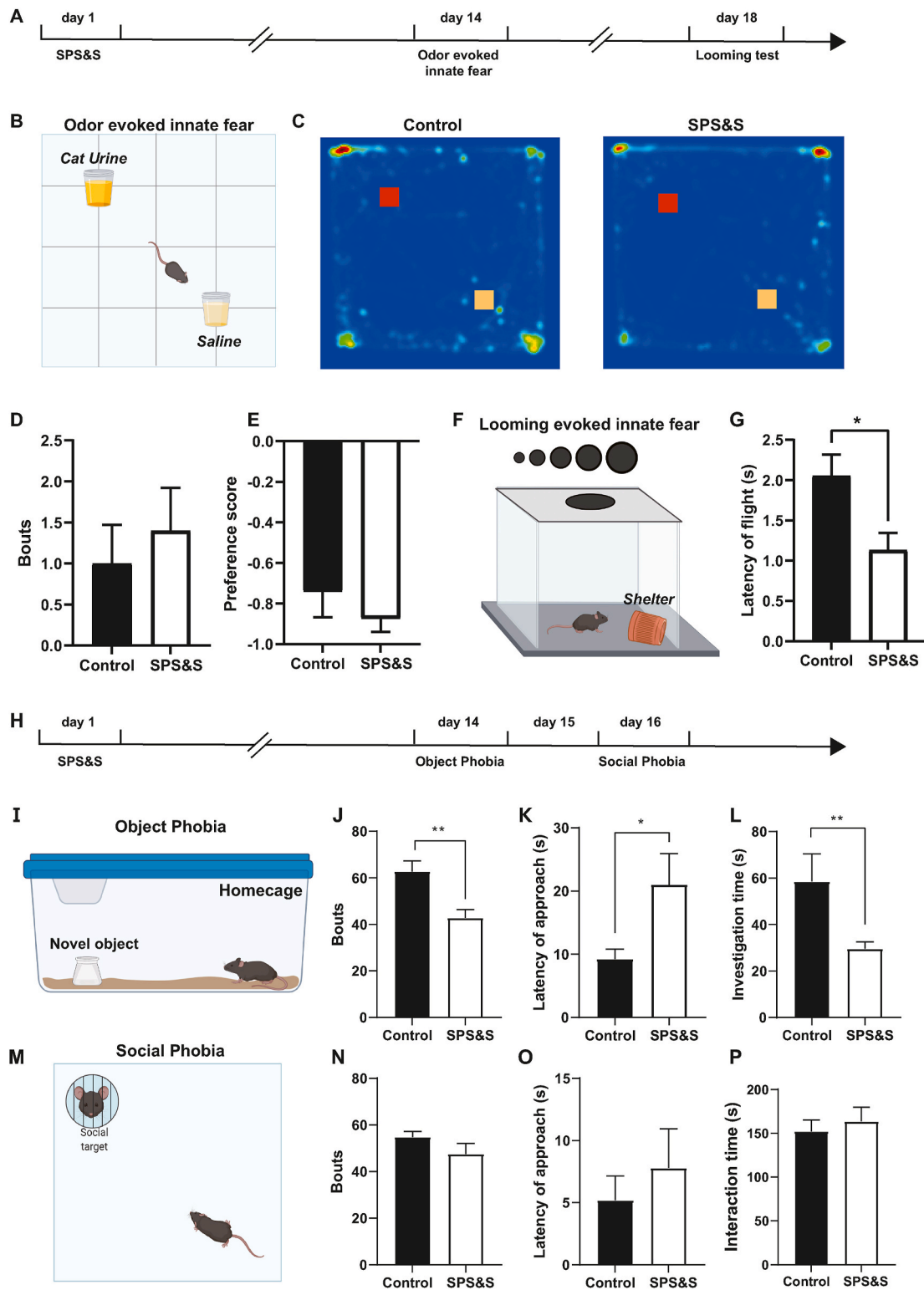
(caption on next page)

Fig. 3. SPS&S mice show increased visual cue-related innate fear and object phobia. A Diagram of the timeline of the odor-evoked innate fear and cue-related innate fear experiment. B Diagram of the odor-evoked innate fear experiment. C Representative heat maps of SPS&S and control mice during the odor-evoked innate fear experiment. D SPS&S mice and control mice exhibited similar interactions with cat urine odor (Mann-Whitney U test, U = 41, P = 0.5122, n = 10 per group). E There was no significant difference in the preference score for cat urine odor between SPS&S mice and control mice (Mann-Whitney U test, U = 47, P = = 0.8172, n = 10 per group). F Diagram of the looming-evoked innate fear experiment. G Compared with control mice, SPS&S mice exhibited a significantly shorter latency time between identifying the dangerous visual stimulation and escaping to shelter (Two-tailed unpaired t-test, t = 2.717, df = 18, P = 0.0141, *P < 0.05, n = 10 per group). H Diagram of the timeline of the object phobia and social phobia experiment. I Diagram of the object phobia experiment. J Compared with control mice, SPS&S mice exhibited fewer explorations of the novel object (Mann-Whitney U test, U = 14, P = 0.0013, **P < 0.01, n = 11 per group). K Compared with control mice, SPS&S mice exhibited a longer latency time to first exploring the novel object (Two-tailed unpaired separate variance estimation t-test, t = 2.267, df = 12.02, P = 0.0427, *P < 0.05, n = 11 per group). L Compared with control mice, SPS&S mice spent less time investigating the novel object (Mann-Whitney U test, U = 17, P = 0.0032, **P < 0.01, n = 11 per group). M Diagram of the social phobia experiment. N There was no significant difference in the number of times the social target was explored between control mice and SPS&S mice (Two-tailed unpaired t-test, t = 0.6124, df = 14.79, P = 0.5496, n = 11 per group). O The latency time for approaching the social target of SPS&S mice and control mice was not significantly different (Mann-Whitney U test, U = 49.50, P = 0.4809, n = 11 per group). P The interaction time with the social target was not significantly different between control mice and SPS&S mice (Two-tailed unpaired t-test, t = 0.4144, df = 22, P = 0.6830, n = 11 per group). *P < 0.05, **P < 0.01.

the analysis, we performed EEG cleaning procedure as described in our previous report (Liu et al., 2016) to exclude potential artifacts. The spectral power was calculated in 0.5-Hz bins (fast Fourier transform with Hamming window) with artifact-free 4-h EEG signals from each animal. The power spectra in the EEG different frequency band were calculated for each animal and averaged across all animals with the same treatment.

2.12. Envelope-to-signal correlation

Envelope-to-signal correlation (ESC) is a cross-correlation between the envelope of high-frequency EEG signal at one recording location and raw low-frequency EEG signal at another location that can evaluate the large-scale cortical cross-frequency interactions across brain regions. A high ESC indicates that the amplitude envelope peaks more reliably at a particular frequency of the amplitude signal (Bruns and Eckhorn 2004). The ESC measure calculates the correlation between the amplitude envelope of the filtered high-frequency signal of FCx (A_{famp}), and the filtered low-frequency signal of the piriform cortex (PCx) (Y_{fph}).

$$ESC_{fph, famp} = r (A_{famp}, Y_{fph}) \qquad (1)$$

A_{famp} denotes the instantaneous amplitude envelope of the higher-frequency signal. Y_{fph} denotes the instantaneous amplitude of the low-frequency signal. r denotes cross-correlation (Onslow et al., 2011).

2.13. Statistical analyses

All statistical analyses were performed in Prism v.6.0 (GraphPad Software, Inc.) and SPSS v.21.0. The normality test was performed by the Shapiro-Wilk test. The homogeneity of variance test was performed by Levene's test. Data that met these two conditions were analyzed using a two-tailed unpaired or paired t-test, one-factor analysis of variance (ANOVA) and repeated-measures ANOVA followed by Tukey's multiple comparisons test. Normally distributed data sets were analyzed with a nonparametric test. Details of particular statistical analyses are presented in Supplementary Table 1.

3. Results

3.1. Fear responses to trauma-related environments in the SPS&S mouse model

According to the Diagnostic and Statistical Manual of Mental Disorders Criteria, Fifth Edition (DSM-V), patients with PTSD tend to have flashbacks to traumatic events and impaired extinction of fear memory related to experienced trauma (Fenster et al., 2018). Therefore, we explored whether SPS&S mice have difficulty in extinguishing fear memory aroused by a trauma-related environment. Numerous studies have shown that mouse freezing time can be used as an important indicator of fear performance (Milad et al., 2009). Therefore, we

conducted the final step of the SPS&S procedure, an inescapable foot electrical stimulation, in Context A (Fig. 1A). Five seconds after the foot shock, SPS&S mice were returned to their cages. Control group mice were placed in Context A but did not receive a foot shock and were returned to their cages after 5 s. On day 14 after model formation, SPS&S mice displayed significantly longer freezing time during a 5-min exploration of Context A than control mice (Fig. 1B). Moreover, when the animals were placed in a novel environment, Context B, SPS&S mice showed no significant difference in fear performance compared with control mice (Fig. 1C). These results suggested that SPS&S mice had impaired extinction of the fear memory associated with the trauma-related environment, relevant to the diagnostic criteria of DSM-V (Fenster et al., 2018).

3.2. Time course of trauma-related fear memory in the SPS&S mouse model

According to previous reports, PTSD model mice have impaired fear memory extinction generated by environmental stimuli (Borghans and Homberg 2015). We explored whether there were obvious behavioral abnormalities in the extinction of fear memory in SPS&S mice. The experimental and control group mice were generated as described above (Fig. 1D). On day 7 after model formation, fear memory extinction of SPS&S mice in response to the trauma-related environmental cue was significantly impaired compared with control mice (Fig. 1E). Next, we explored whether this alteration could be observed at a later timepoint. With the same protocols, the fear memory generated by the trauma-related environmental cue in SPS&S mice was slightly higher on day 14 than day 7. In comparison, the fear level of control mice was still relatively low (Fig. 1F). Thus, in this set of short- and long-term memory experiments, SPS&S model mice demonstrated impaired fear memory extinction observed in PTSD patients.

3.3. Fear memory formation and extinction in the SPS&S mouse model

Since SPS&S mice showed abnormal fearful responses to the trauma-related context, we explored possible fear memory formation and extinction problems in SPS&S model mice. We applied a classic cue-plus-contextual fear conditioning paradigm, coupling the memory of auditory cues and foot shocks different from the contextual fear conditioning, to assess the formation and extinction of fear memory (Fig. 2A). During the first day of training, the baseline freezing time of SPS&S mice was significantly higher than control mice. After each auditory cue and simultaneous foot shock, the fear level of SPS&S mice was also higher than control mice, indicating that SPS&S mice were more likely to establish fear memory during auditory cue-related fear training (Fig. 2B). On the second day of training, we placed the mice in a novel context and used the same auditory cue to evaluate fear performance after 3 min of adaptation. The freezing time of SPS&S mice during the 3-min period was significantly higher than control mice (Fig. 2C),
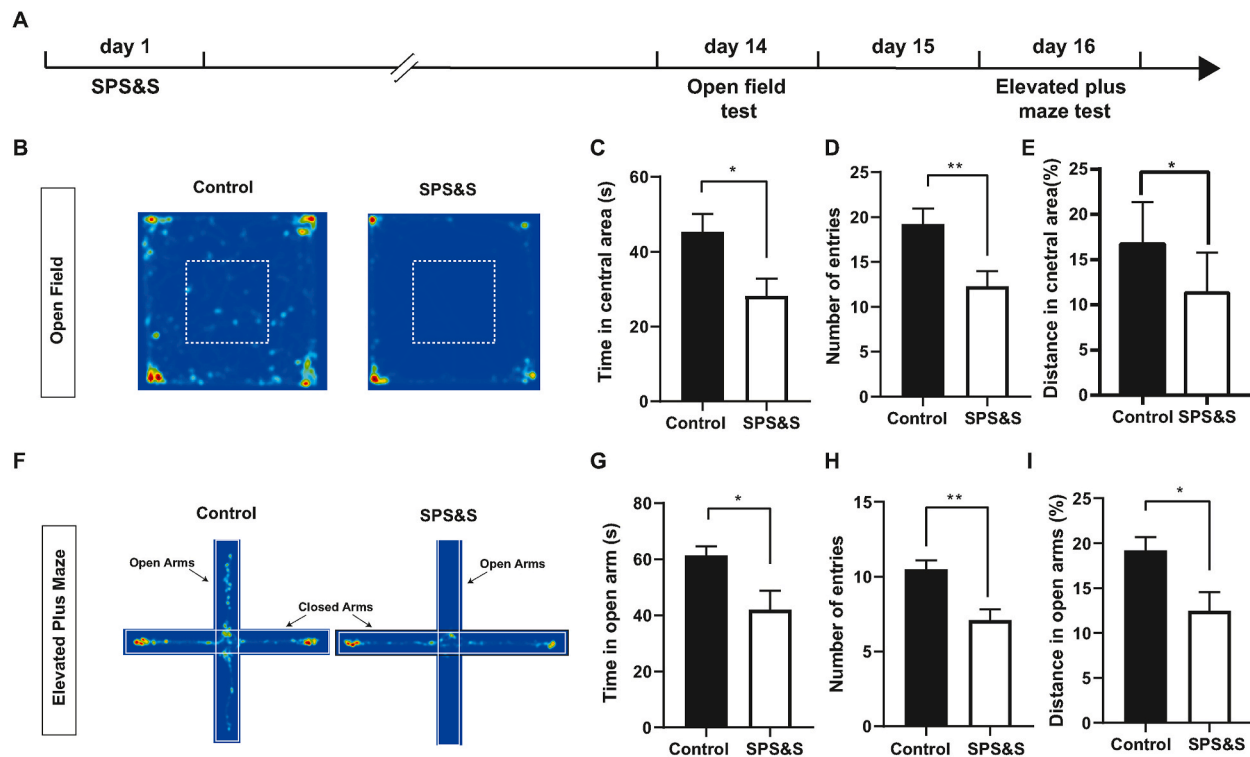
Fig. 4. SPS&S mice show increased anxiety. A Diagram of the timeline of the open field test and elevated plus maze test. B Representative heat maps of open field test. C Compared with control mice, SPS&S mice spent less time in the central area (Two-tailed unpaired *t*-test, t = 2.558, df = 18, *P* = 0.0198, n = 10 per group). D Compared with control mice, SPS&S mice entered the central area less frequently (Two-tailed unpaired *t*-test, t = 2.883, df = 18, *P* = 0.0099, n = 10 per group). E Compared with control mice, SPS&S mice traveled less distances in the central area (Two-tailed unpaired *t*-test, t = 2.625, df = 18, *P* = 0.0172, n = 10 per group). *P < 0.05, **P < 0.01. F Representative heat maps of elevated plus maze test. G Compared with control mice, SPS&S mice spent significantly less time in the open arms (Two-tailed unpaired separate variance estimation *t*-test, t = 2.561, df = 12.88, *P* = 0.0238, n = 10 per group). H Compared with control mice, SPS&S mice entered the open arms of the elevated plus maze less frequently (Two-tailed unpaired *t*-test, t = 3.666, df = 18, *P* = 0.0018, n = 10 per group). I Compared with control mice, SPS&S mice traveled significantly shorter distances in the open arms (Two-tailed unpaired *t*-test, t = 2.605, df = 18, *P* = 0.0179, n = 10 per group).

indicating a higher level of auditory cue-induced fear. These results indicated that the animals established fear memory more easily after SPS&S stress.

Following training completion, we assessed the extinction and retrieval of fear memory. Before the memory extinction experiments, the fear memory level generated by auditory cues in SPS&S mice was higher than in control mice. During the extinction process, the freezing time of both SPS&S and control mice decreased. However, during the retrieval experiment on the following day, the freezing time of SPS&S mice was still higher than control mice (Fig. 2D). These results demonstrated that SPS&S mice had a strong resistance and showed defects in fear memory extinction caused by auditory cues.

3.4. Innate fearful behaviors in the SPS&S mouse model

Besides the learned fear, PTSD patients show increased instinctive fear of certain clinical stimuli (Braquehais and Sher 2010; Taylor et al., 2020). To investigate whether the model mice also show alterations in innate fearful behaviors following SPS&S stress, we measured the fear performance induced by cat urine odor and visual looming (Fig. 3A). For the odor-induced fearful behaviors (Fig. 3B), control mice spent less time exploring the cat urine odor area than the saline odor area, as shown in the heat map in Fig. 3C, consistent with their physiological condition (Schutz et al., 2014). There was no significant difference in bouts of sniffing and preference score between SPS&S and control mice (Fig. 3D and E). We conducted a looming test to assess visual cue-induced innate fear that investigates the fearful responses caused by the appearance of a predator's rapidly approaching shadow above the mouse (Fig. 3F). The time between the mouse realizing the potential

danger and entering shelter to avoid the attack could reflect its fear level, with a shorter time indicating higher fear (Zhou et al., 2019). We found that the flight latency was significantly shorter for SPS&S mice than control mice (Fig. 3G), showing that the SPS&S mouse model could mimic the enhanced innate fear induced by visual stimuli observed in PTSD patients.

3.5. Phobia behaviors in the SPS&S mouse model

PTSD and phobias commonly co-occur in clinical practice, and phobias aggravate the core PTSD symptoms (Orsillo et al., 1996). We tested their phobia of novel objects and social targets to assess whether SPS&S mice also show relevant phobia behaviors (Fig. 3H). In the object phobia test, we found that the number of mice exploring the novel object was significantly lower, the latency of approaching was higher, and the exploration time was significantly less in SPS&S mice than control mice (Fig. 3J-L). In the social phobia test, there was no significant difference in the number of social contacts, the latency of approaching the social target, or overall social time between the experimental and control mice (Fig. 3N-P). These results indicated that the SPS&S stress could recapitulate the concomitant object phobia of PTSD patients but not the social phobia behaviors.

3.6. Anxiety behaviors in the SPS&S mouse model

Anxiety disorders have shown high morbidity in PTSD patients compared with healthy people (Kalin 2021). To assess whether the model mice also display anxiety-like behaviors after SPS&S stress, we used open field assays and the elevated plus maze to measure anxiety
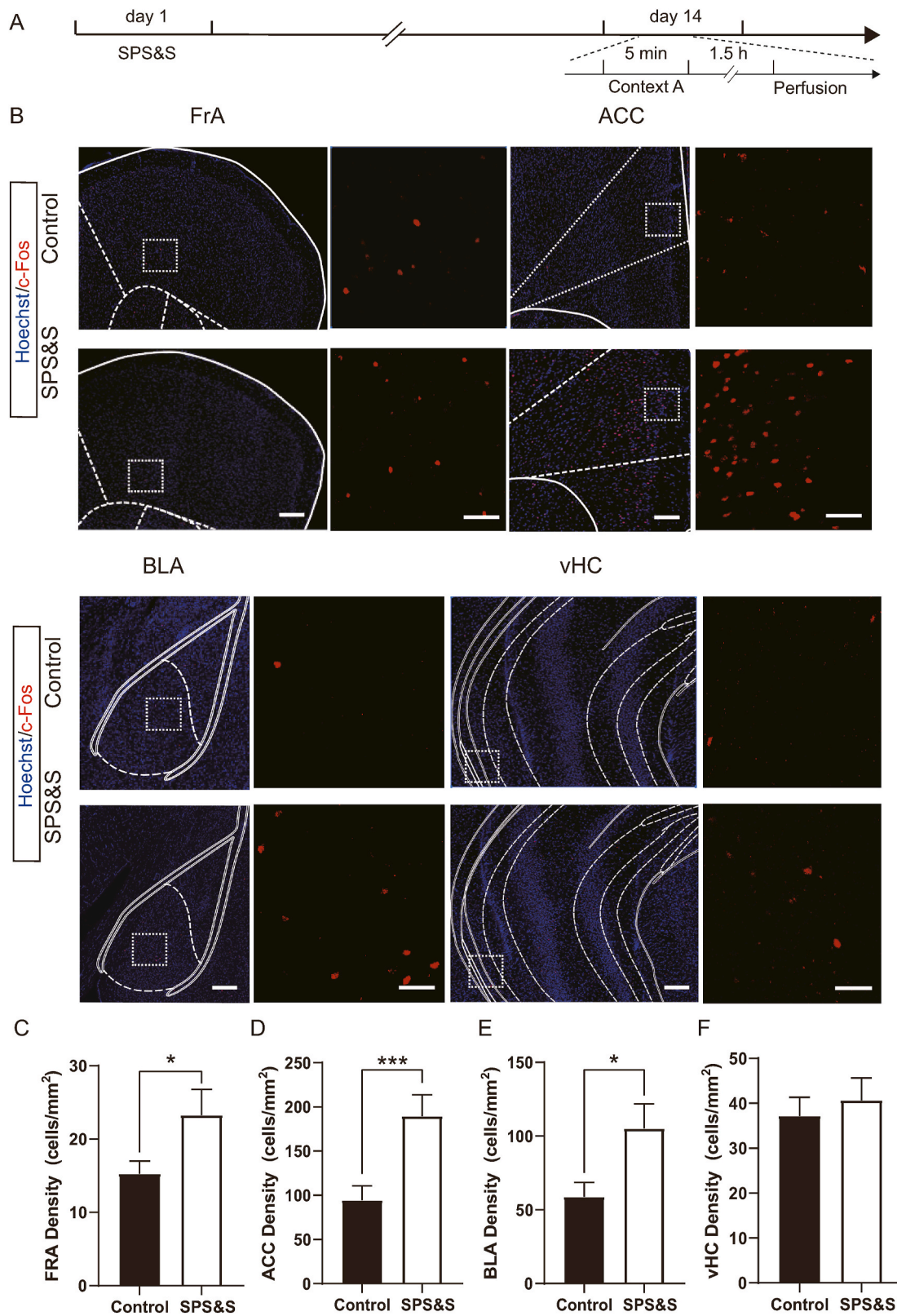
(caption on next page)

Fig. 5. SPS&S mice show wide neuronal overactivation in fear-related brain regions. A Diagram of the timeline of the perfusion the animals. B Representative confocal images of FrA, ACC, BLA, and vHC sections stained for c-Fos in SPS&S mice and control mice. Images on the right of each brain region are high-magnification images of the boxed area. Scale bar for low-magnification images = 200 μm, Scale bar for high-magnification images = 50 μm. C Compared with control mice, SPS&S mice exhibited a higher density of cells immunoreactive for c-Fos in the FrA (Two-factor ANOVA, $F_{between\ group}$ = 4.928, df1 = 1, df2 = 12, $P_{between\ group}$ = 0.0465; $F_{between\ animal}$ = 2.725, df1 = 2, df2 = 12, $P_{between\ animal}$ = 0.1058; n = 10 slices from 3 mice (Control), n = 7 slices from 3 mice (SPS&S)). D Compared with control mice, SPS&S mice exhibited a higher density of cells immunoreactive for c-Fos in the ACC (Two-factor ANOVA, $F_{between\ group}$ = 16, df1 = 1, df2 = 23, $P_{between\ group}$ = 0.0006; $F_{between\ animal}$ = 3.315, df1 = 2, df2 = 23, $P_{between\ animal}$ = 0.0625; n = 12 slices from 3 mice (Control), n = 17 slices from 3 mice (SPS&S)). E Compared with control mice, SPS&S mice exhibited a higher density of cells immunoreactive for c-Fos in the BLA (Two-factor ANOVA, $F_{between\ group}$ = 5.353, df1 = 1, df2 = 14, $P_{between\ group}$ = 0.0364; $F_{between\ animal}$ = 0.4939, df1 = 2, df2 = 14, $P_{between\ animal}$ = 0.6205; n = 10 slices from 3 mice (Control), n = 10 slices from 3 mice (SPS&S)). F SPS&S mice and control mice exhibited similar densities of cells immunoreactive for c-Fos in the vHC (Two-factor ANOVA, $F_{between\ group}$ = 0.9632, df1 = 1, df2 = 11, $P_{between\ group}$ = 0.3475; $F_{between\ animal}$ = 0.3539, df1 = 2, df2 = 11, $P_{between\ animal}$ = 0.7097; n = 7 slices from 3 mice (Control), n = 11 slices from 3 mice (SPS&S)). $*P < 0.05$, $***P < 0.001$.

levels (Fig. 4A). In the open field test, the control mice widely explored the central area, whereas the SPS&S mice mostly stayed in the corner of the open field. The SPS&S mice spent less time, traveled less distance in the central area, and entered the central area less often (Fig. 4C–E). In the elevated plus-maze test, control mice spent abundant time exploring the open arms, closed arms, and central area. In contrast, SPS&S mice spent less time exploring the open arms, showed fewer entries, and traveled shorter distances in the open arms (Fig. 4G–I). Based on these results, we concluded that SPS&S mice showed significant anxiety-like behaviors, meeting the relevant diagnostic criteria of PTSD from DSM-V.

3.7. Neural and glial activation in the SPS&S mouse model

Malfunction of some brain regions, including the hippocampus and amygdala, has been implicated in PTSD-related core symptoms., We used *c-Fos*, an immediate early gene rapidly induced by a broad range of stimuli, to assess the PTSD-related function in brain regions in model mice. Following stimulation of the traumatic context, the number of c-Fos-expressing neurons was widely increased in fear-related regions. In the frontal association cortex (FrA), anterior cingulate cortex (ACC), and basolateral amygdala (BLA), the number of c-Fos-positive neurons was significantly higher than in control mice. However, in the ventral hippocampus (vHC), there was no difference between SPS&S and control mice (Fig. 5).

Besides neuronal activation, an abnormal neuroimmune state reflecting glial activation has also been observed in postmortem PTSD patients. We used GFAP and IBa1 as markers for mature astrocytes and microglia. The expression level of GFAP was increased in the ACC, BLA, and vHC of SPS&S mice compared with control mice, indicating that astrocytes were significantly activated in these regions (Fig. 6B–F). Also, the number of microglia labeled by IBa1 in the FrA and ACC was significantly increased in SPS&S mice relative to control mice, denoting activation of microglia in these regions (Fig. 6G–K). These results suggested that the SPS&S mouse model showed wide neural and glial activation induced by the trauma-related environment, recapitulating the dysfunction of fear-associated brain regions in PTSD patients.

3.8. EEG power spectra and coupling relationships of frontal and PCx) in the SPS&S mouse model

It was previously reported that the delta, theta, and alpha power spectra in PTSD patients were suppressed compared to healthy people during eye-open states (Newson and Thiagarajan 2018). We investigated whether SPS&S mice exhibited the same suppressed power spectra by recording power spectra with the screw implanted on the skull above the FCx or PCx while mice were freely moving. The EEG signals of SPS&S mice showed widely decreased power spectra compared with control mice at both FCx and PCx recording sites. At the FCx site, while the delta, theta, and alpha power spectra were weaker in SPS&S mice than control mice, there was little difference in the beta and gamma power spectra (Fig. 7B). Interestingly, at the PCx site, SPS&S mice showed significantly decreased delta and theta power spectra than control mice and displayed little changes in the alpha, beta, and gamma power spectra (Fig. 7D).

Furthermore, we investigated whether there was a change in the correlation between FCx and PCx with SPS&S stress. Cross-frequency coupling was examined using a comodugram to determine the extent to which a high-frequency (30–80 Hz) amplitude envelope was modulated by a low-frequency (0–30 Hz) raw signal. The envelope-to-signal correlation (ESC) was employed to quantify the cross-frequency coupling strength (Bruns and Eckhorn 2004; Onslow et al., 2011). We found that the gamma bands (40–70 Hz) at PCx were strongly coupled with low-frequency (4–10 Hz) oscillations at FCx (Fig. 7E and F). However, in SPS&S mice, ESC values were lower than the control mice (Fig. 7E and F). The mean ESC strength as a function of envelope frequency or amplitude signal frequency was also calculated. The average ESC of envelope frequency in SPS&S mice was significantly lower than control mice in both low frequency and high frequency (Fig. 7G and H). These results indicated that SPS&S mice were a good mimic of patients with PTSD in terms of their altered EEG power spectra. Additionally, the weak FCx–PCx coupling might contribute to PTSD symptoms.

4. Discussion

Dissecting the mechanisms of PTSD in animal models is challenging because of the complexity of the processes underlying its initiation and manifestation. Appropriate animal models are expected to display critical aspects of PTSD etiology, symptomatology, and treatment response (Daskalakis et al., 2013). So far, diverse PTSD stress rodent models have been generated (Ferland-Beckham et al., 2021). SPS is one of the most well-established stress models and is especially stable in rats (Fan et al., 2021). Other stress protocols have also been applied in many studies, each with its own advantages. For example, predator-based psychosocial stress (PPS) induces significant PTSD-like anxiety behaviors and impaired fear extinction. PPS uses environmental stressors, including constant changing of housing pairs, exposure to the risk of predators, and immobilization (Zoladz et al., 2012).

In recent years, genetically modified animals have been used since the homogeneity of these models can facilitate mechanistic studies. In this context, 5-HT1A receptor knockout mice show severe anxiety and enhanced fear extinction phenotypes (Parks et al., 1998), and Pet-1 knockout mice display anxiety, aggression, and excessive fear response (Hendricks et al., 2003). Though these animal models exhibit PTSD-like behaviors and are useful tools to help understand the relationship between PTSD and various genes, the lack of interplay with environmental and stress factors makes it hard to translate the preclinical data to complex clinical practice.

Herein, we used a modified SPS&S protocol to induce PTSD-like behaviors in mice. We found that SPS&S mice exhibit robust PTSD symptoms, including enhanced fear response to traumatic and specific non-traumatic cues, elevated anxiety behaviors, object phobias, and enhanced fear retrieval. Notably, social phobia is commonly observed in PTSD patients (Santiago et al., 2013); however, SPS&S mice with the current behavioral paradigm did not display abnormal social phobia. This could be due to the selection of stimulus animals and the social hierarchy of test animals (Zhou et al., 2017). Interpretation of this set of data necessitates caution and needs further exploration. Besides these
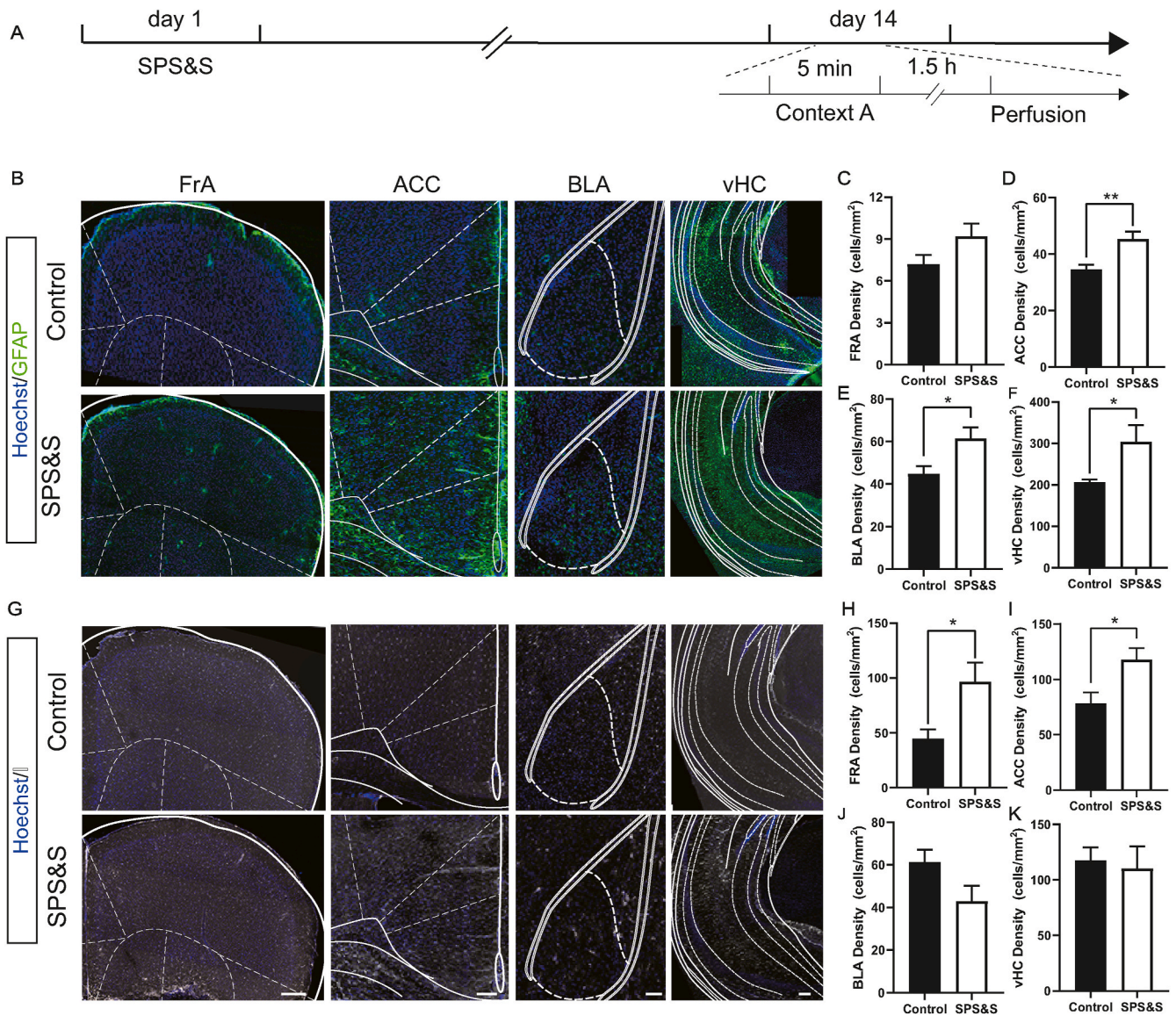
Fig. 6. SPS&S mice show glial activation in fear-related brain. A Diagram of the timeline of the perfusion the animals. B Representative confocal images of sections stained for GFAP from SPS&S mice and control mice. C The density of cells immunoreactive for GFAP in the FRA was similar between SPS&S mice and control mice (Two-factor ANOVA, $F_{between\ group}$ = 2.644, df1 = 1, df2 = 8, $P_{between\ group}$ = 0.1426; $F_{between\ animal}$ = 1.347, df1 = 2, df2 = 8, $P_{between\ animal}$ = 0.3131; n = 8 slices from 3 mice (Control), n = 6 slices from 3mice (SPS&S)). D Compared with control mice, SPS&S mice exhibited a higher density of cells immunoreactive for GFAP in the ACC (Two-factor ANOVA, $F_{between\ group}$ = 13.96, df1 = 1, df2 = 13, $P_{between\ group}$ = 0.0025; $F_{between\ animal}$ = 1.291, df1 = 2, df2 = 13, $P_{between\ animal}$ = 0.3097; n = 11 slices from 3 mice (Control), n = 8 slices from 3 mice (SPS&S)). E Compared with control mice, SPS&S mice exhibited a higher density of cells immunoreactive for GFAP in the BLA (Two-factor ANOVA, $F_{between\ group}$ = 7.77, df1 = 1, df2 = 13, $P_{between\ group}$ = 0.0154; $F_{between\ animal}$ = 1.548, df1 = 2, df2 = 13, $P_{between\ animal}$ = 0.2495; n = 11 slices from 3 mice (Control), n = 8 slices from 3 mice (SPS&S)). F Compared with control mice, SPS&S mice exhibited a higher density of cells immunoreactive for GFAP in the vHC (Two-factor ANOVA, $F_{between\ group}$ = 8.173, df1 = 1, df2 = 11, $P_{between\ group}$ = 0.0155; $F_{between\ animal}$ = 1.902, df1 = 2, df2 = 11, $P_{between\ animal}$ = 0.1952; n = 9 slices from 3 mice (Control), n = 8 slices from 3 mice (SPS&S)). G Representative confocal images of sections stained for IBA1 from SPS&S mice and control mice. H Compared with control mice, SPS&S mice exhibited a higher density of cells immunoreactive for IBA1 in the FrA (Two-factor ANOVA, $F_{between\ group}$ = 8.717, df1 = 1, df2 = 14, $P_{between\ group}$ = 0.0105; $F_{between\ animal}$ = 1.115, df1 = 2, df2 = 14, $P_{between\ animal}$ = 0.3553; n = 12 slices from 3 mice (Control), n = 8 slices from 3 mice (SPS&S)). I Compared with control mice, SPS&S mice exhibited a higher density of cells immunoreactive for IBA1 in the ACC (Two-factor ANOVA, $F_{between\ group}$ = 7.351, df1 = 1, df2 = 27, $P_{between\ group}$ = 0.0115; $F_{between\ animal}$ = 0.1202, df1 = 2, df2 = 27, $P_{between\ animal}$ = 0.8872; n = 19 slices from 3 mice (Control), n = 14 slices from 3 mice (SPS&S)). J The density of cells immunoreactive for IBA1 in the BLA was similar in SPS&S mice and control mice (Two-factor ANOVA, $F_{between\ group}$ = 4.694, df1 = 1, df2 = 11, $P_{between\ group}$ = 0.0531; $F_{between\ animal}$ = 0.466, df1 = 2, df2 = 11; $P_{between\ animal}$ = 0.6394; n = 10 slices from 3 mice (Control), n = 7 slices from 3 mice (SPS&S)). K Compared with control mice, SPS&S mice exhibited a higher density of cells immunoreactive for IBA1 in the vHC (Two-factor ANOVA, $F_{between\ group}$ < 0.001, df1 = 1, df2 = 22, $P_{between\ group}$ = 0.9941; $F_{between\ animal}$ = 2.514, df1 = 2, df2 = 22; $P_{between\ animal}$ = 0.1040; n = 10 slices from 3 mice (Control), n = 7 slices from 3 mice (SPS&S)). *P < 0.05, **P < 0.01. Scale bar = 100 μm.

behavioral symptoms, SPS&S mice also showed neural activation in PTSD-vulnerable brain regions, neuroimmune responses, and abnormal EEG phenotypes. These profiling studies provide a clearer picture of the mouse model and evidence for its future use in screening effective therapeutic strategies and investigating the underlying PTSD

mechanisms. However, to recapitulate the cognitive impairments observed in patients with PTSD, the development of primate models might be necessary for future research. Additionally, in this study, all data were collected from male animals. Since the gender difference might lead to distinct behavioral and neurobiological phenotypes,
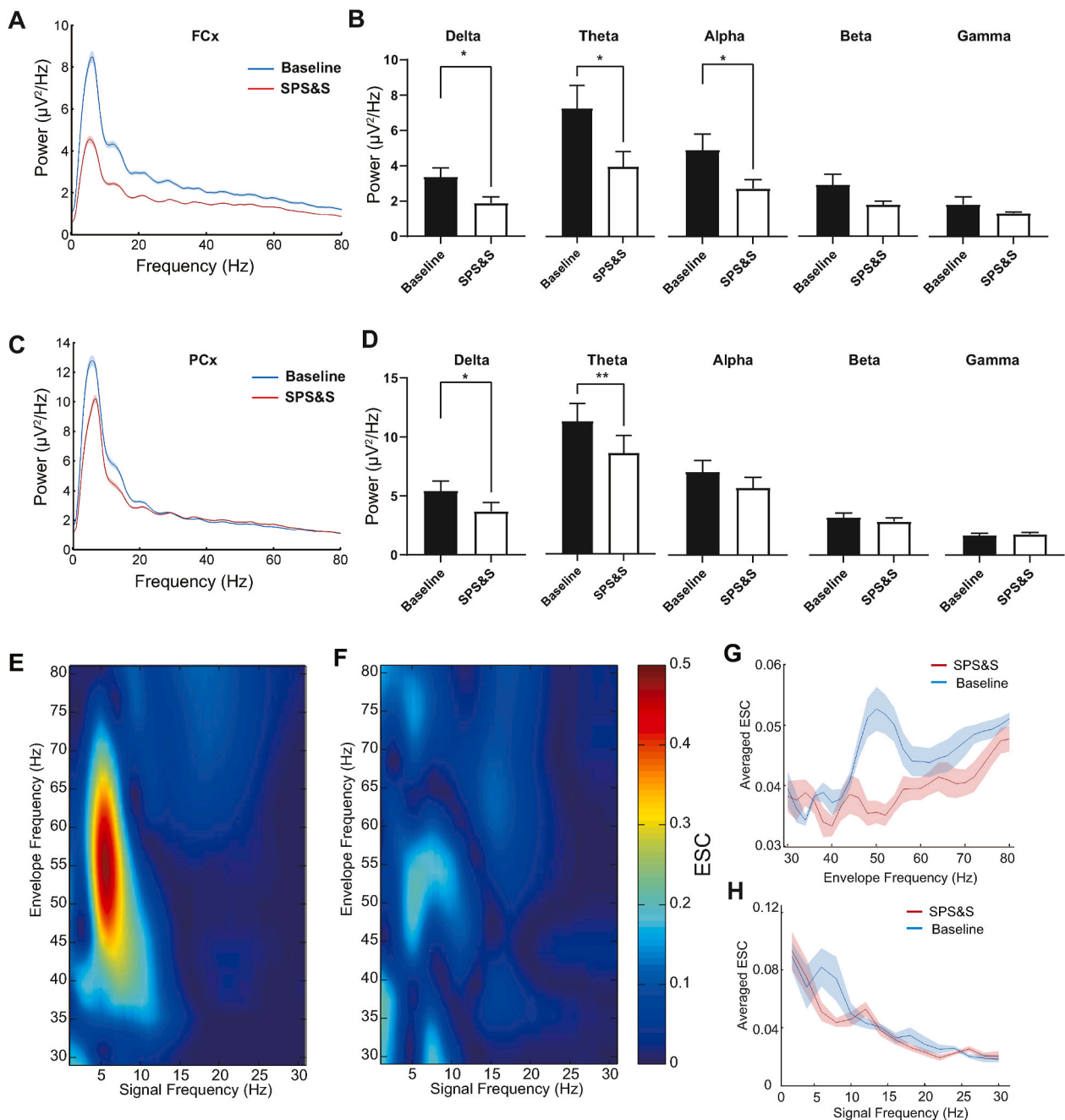
Fig. 7. SPS&S mice show decreased EEG power spectra and FCx-PCx coupling. A Example power spectra in the FCx collected over 4 h with eyes open. b) Compared with control mice, SPS&S mice exhibited decreased delta (Two-tailed paired *t*-test, t = 0.5090, df = 3, *P* = 0.0147, n = 4 per group), theta (Two-tailed paired *t*-test, t = 4.664, df = 3, *P* = 0.0186, n = 4 per group), and alpha (Two-tailed paired *t*-test, t = 4.073, df = 3, *P* = 0.0267, n = 4 per group) power spectra in the FCx. There was little difference in the beta (Two-tailed paired *t*-test, t = 2.292, df = 3, *P* = 0.1058, n = 4 per group) and gamma (Two-tailed paired separate variance estimation *t*-test, t = 0.9475, df = 3, *P* = 0.4133, n = 4 per group). B Power spectra of SPS&S mice and control mice. C Example power spectra in the PCx collected over 4 h with eyes open. Both SPS&S mice and control mice showed peak power at theta (peak at 6 Hz), while SPS&S mice exhibited widely decreased power spectra compared with control mice. D Compared with control mice, SPS&S mice exhibited decreased delta (Two-tailed paired *t*-test, t = 5.174, df = 3, *P* = 0.0140, n = 4 per group) and theta (Two-tailed paired *t*-test, t = 10.77, df = 3, *P* = 0.0017, n = 4 per group) power spectra in the PCx. SPS&S mice and control mice exhibited similar alpha (Two-tailed paired *t*-test, t = 2.627, df = 3, *P* = 0.0785, n = 4 per group), beta (Two-tailed paired *t*-test, t = 1.892, df = 3, *P* = 0.1548, n = 4 per group), and gamma (Two-tailed paired separate variance estimation *t*-test, t = 0.4021, df = 3, *P* = 0.7146, n = 4 per group) power spectra. E Example envelope-to-signal comodulograms obtained from EEGs between envelopes of high-frequency signals (y-axis) at FCx and raw low-frequency signals at PCx (x-axis) at baseline. The pseudocolor scale represents the ESC values shown on the right; warm colors indicate stronger modulation. Note the prominent modulation of slow gamma (40–70 Hz) peaks. F Example envelope-to-signal comodulograms obtained from EEGs between envelopes of high-frequency signals (y-axis) at FCx and raw low-frequency signals at PCx (x-axis) in SPS&S mice. Note the prominent modulation of slow gamma (40–70 Hz) peaks. G Mean ESC strength (average ESC) as a function of envelope frequency. SPS&S mice exhibited significantly weaker ESC values than control mice (Repeated measurement ANOVA, $F_{between\ group}$ = 6.545, df1 = 1, df2 = 4.022, $P_{between\ group}$ = 0.001; $F_{within\ group}$ = 6.515, df1 = 1, df2 = 6, $P_{withingroup}$ = 0.043; *P < 0.05, n = 4 per group). H Mean ESC strength (average ESC) as a function of amplitude signal frequency. SPS&S mice exhibited little difference from control mice (Repeated measurement ANOVA, $F_{between\ group}$ = 16.206, df1 = 1, df2 = 14, $P_{between\ group}$ < 0.0001; $F_{within\ group}$ = 1.340, df1 = 1, df2 = 6, $P_{withingroup}$ = 0.277; n = 4 per group). *P < 0.05, **P < 0.01. . (For interpretation of the references to color in this figure legend, the reader is referred to the Web version of this article.)

further characterization of different genders of animals is needed in the future.

Evidence from human studies suggests that the vulnerable brain regions associated with PTSD symptoms are the ACC, amygdala, and hippocampus, involved in the formation and retrieval of emotion and fear memory (Stout et al., 2019; Belleau et al., 2020; Dark et al., 2021; Harnett et al., 2021). Using MRI to study structural changes in patients with PTSD, previous studies found reduced volumes of the hippocampus and ACC (Yamasue et al., 2003; Kitayama et al., 2005; Dark et al., 2021). fMRI studies reported hyperactivity in the amygdala (Koch et al., 2016), while ACC results were not consistent across different studies. Several groups reported excessive ACC activities in PTSD patients compared with healthy subjects (Hayes et al., 2012; Zweerings et al., 2018), but another study showed a hypo-functional ACC in fear conditions (Shin et al., 2001). Consistent with these clinical findings, we observed the neuronal activity of SPS&S mice in these brain regions and an increased number of c-Fos-expressing neurons, indicating that the SPS&S mouse model recapitulated the neuronal abnormalities in PTSD-vulnerable brain regions observed in patients.

A pioneering human study found that exposure to traumatic events could also lead to inflammation in the peripheral immune system (Eraly et al., 2014). C-reactive protein, interleukin 6, interleukin 1β, and tumor necrosis factor α were found to be increased in blood samples from PTSD patients, indicating an excessive immune state in the peripheral system (Tursich et al., 2014; Friend et al., 2020). Furthermore, evidence from positron emission tomography and postmortem transcriptomic studies revealed that abnormal glial cells were related to neuroimmune activation in the brain (Bhatt et al., 2020). Preclinical studies in PTSD rodent models also observed increased astrocyte- and microglia-specific proteins and cell-surface markers (Tynan et al., 2010; Xia et al., 2013; Feng et al., 2015), suggesting neuroimmune responses to PTSD-related stress. We also observed activation of astrocytes and microglia in PTSD-related brain regions, indicating that our mouse model could potentially mimic the neuroimmune pathophysiology and symptomatology in the brain.

EEG is used to inform clinical diagnosis and treatment effectiveness and could potentially serve as an unbiased biomarker for PTSD (Newson and Thiagarajan 2018). Multiple studies have assessed the absolute power of various frequency bands (alpha, beta, gamma, theta, and delta waves) in PTSD patients during resting state conditions (eyes open and closed) (Shankman et al., 2008; Kemp et al., 2010; Todder et al., 2012; Imperatori et al., 2014). In these studies, all frequency bands were decreased under eyes open conditions with delta, theta, and alpha bands displaying significant differences. Significantly, we found similar results in SPS&S mice. The powers of the delta, theta, and alpha bands were reduced after stress, while the beta and gamma bands did not significantly change. Also, previous functional imaging studies have found that the connectivity between cortical regions was abnormal in PTSD patients (Philippi et al., 2021). Consistent with these observations, EEG data collected from the frontal and piriform areas revealed an impaired EEG coupling relationship, which could be a potential clinical readout for future therapeutic evaluations. These results suggested that the PTSD mouse model also mimicked the EEG phenotypes observed in the clinic, indicating the possibility of using EEG as an additional assessment to study PTSD in rodents.

In conclusion, we systematically explored the translational relevance of a modified SPS&S mouse model for PTSD. We found that this mouse model recapitulated PTSD-like behavioral abnormalities, including elevated fear responses to traumatic and specific non-traumatic cues, aberrant innate fear behaviors, phobias, and anxiety behaviors. Additionally, this model showed increased neural activation in PTSD-vulnerable brain regions, excessive neuroimmune responses, and reduced EEG powers of the delta, theta, and alpha bands. These results indicated that the SPS&S mouse model has translational significance for preclinical studies, especially for developing biomarkers and effective pharmacotherapy strategies for PTSD.

Declaration of competing interest

The authors declare that they have no known competing financial interests or personal relationships that could have appeared to influence the work reported in this paper.

CRediT authorship contribution statement

Kaiwen Xi: Investigation, Formal analysis, Writing – original draft. **Xin Huang:** Investigation, Formal analysis, Writing – original draft. **Tiaotiao Liu:** Investigation, Methodology, Formal analysis. **Yang Liu:** Methodology. **Honghui Mao:** Investigation, Formal analysis. **Mengmeng Wang:** Investigation. **Dayun Feng:** Methodology. **Wenting Wang:** Methodology, Writing – review & editing. **Baolin Guo:** Conceptualization, Methodology, Writing – review & editing, Supervision. **Shengxi Wu:** Conceptualization, Writing – review & editing, Supervision, Funding acquisition.

Data availability

Data will be made available on request.

Appendix A. Supplementary data

Supplementary data to this article can be found online at https://doi.org/10.1016/j.ynstr.2021.100391.

Declaration of competing interest

The authors declare that they have no known competing financial interests or personal relationships that could have appeared to influence the work reported in this paper.

References

Belleau, E.L., Ehret, L.E., Hanson, J.L., Brasel, K.J., Larson, C.L., deRoon-Cassini, T.A., 2020. Amygdala functional connectivity in the acute aftermath of trauma prospectively predicts severity of posttraumatic stress symptoms. Neurobiol. Stress 12, 100217. https://doi.org/10.1016/j.ynstr.2020.100217.

Bhatt, S., Hillmer, A.T., Girgenti, M.J., Rusowicz, A., Kapinos, M., Nabulsi, N., Huang, Y., Matuskey, D., Angarita, G.A., Esterlis, I., Davis, M.T., Southwick, S.M., Friedman, M. J., Traumatic Stress Brain Study, G., Duman, R.S., Carson, R.E., Krystal, J.H., Pietrzak, R.H., Cosgrove, K.P., 2020. PTSD is associated with neuroimmune suppression: evidence from PET imaging and postmortem transcriptomic studies. Nat. Commun. 11 (1), 2360. https://doi.org/10.1038/s41467-020-15930-5.

Borghans, B., Homberg, J.R., 2015. Animal models for posttraumatic stress disorder: an overview of what is used in research. World J. Psychiatr. 5 (4), 387–396. https://doi.org/10.5498/wjp.v5.i4.387.

Braquehais, M.D., Sher, L., 2010. Posttraumatic stress disorder in war veterans: a discussion of the Neuroevolutionary Time-depth Principle. J. Affect. Disord. 125 (1–3), 1–9. https://doi.org/10.1016/j.jad.2009.08.008.

Bruns, A., Eckhorn, R., 2004. Task-related coupling from high- to low-frequency signals among visual cortical areas in human subdural recordings. Int. J. Psychophysiol. 51 (2), 97–116. https://doi.org/10.1016/j.ijpsycho.2003.07.001.

Bryant, R.A., Williamson, T., Erlinger, M., Felmingham, K.L., Malhi, G., Hinton, M., Williams, L., Korgaonkar, M.S., 2021. Neural activity during response inhibition associated with improvement of dysphoric symptoms of PTSD after trauma-focused

psychotherapy-an EEG-fMRI study. Transl. Psychiatry 11 (1), 218. https://doi.org/10.1038/s41398-021-01340-8.

Chauke, M., de Jong, T.R., Garland Jr., T., Saltzman, W., 2012. Paternal responsiveness is associated with, but not mediated by reduced neophobia in male California mice (Peromyscus californicus). Physiol. Behav. 107 (1), 65–75. https://doi.org/10.1016/j.physbeh.2012.05.012.

Dark, H.E., Harnett, N.G., Knight, A.J., Knight, D.C., 2021. Hippocampal volume varies with acute posttraumatic stress symptoms following medical trauma. Behav. Neurosci. 135 (1), 71–78. https://doi.org/10.1037/bne0000419.

Daskalakis, N.P., Yehuda, R., Diamond, D.M., 2013. Animal models in translational studies of PTSD. Psychoneuroendocrinology 38 (9), 1895–1911. https://doi.org/10.1016/j.psyneuen.2013.06.006.

Eraly, S.A., Nievergelt, C.M., Maihofer, A.X., Barkauskas, D.A., Biswas, N., Agorastos, A., O'Connor, D.T., Baker, D.G., Marine Resiliency Study, T., 2014. Assessment of plasma C-reactive protein as a biomarker of posttraumatic stress disorder risk. JAMA Psychiatr. 71 (4), 423–431. https://doi.org/10.1001/jamapsychiatry.2013.4374.

Fan, Z., Chen, J., Li, L., Wang, H., Gong, X., Xu, H., Wu, L., Yan, C., 2021. Environmental enrichment modulates HPA axis reprogramming in adult male rats exposed to early adolescent stress. Neurosci. Res. https://doi.org/10.1016/j.neures.2021.04.007.

Feng, D., Guo, B., Liu, G., Wang, B., Wang, W., Gao, G., Qin, H., Wu, S., 2015. FGF2 alleviates PTSD symptoms in rats by restoring GLAST function in astrocytes via the JAK/STAT pathway. Eur. Neuropsychopharmacol 25 (8), 1287–1299. https://doi.org/10.1016/j.euroneuro.2015.04.020.

Feng, D.Y., Guo, B.L., Liu, G.H., Xu, K., Yang, J., Tao, K., Huang, J., Wang, L.Y., Wang, W., Wu, S.X., 2020. Nerve growth factor against PTSD symptoms: preventing the impaired hippocampal cytoarchitectures. Prog. Neurobiol. 184, 101721. https://doi.org/10.1016/j.pneurobio.2019.101721.

Fenster, R.J., Lebois, L.A.M., Ressler, K.J., Suh, J., 2018. Brain circuit dysfunction in post-traumatic stress disorder: from mouse to man. Nat. Rev. Neurosci. 19 (9), 535–551. https://doi.org/10.1038/s41583-018-0039-7.

Ferland-Beckham, C., Chaby, L.E., Daskalakis, N.P., Knox, D., Liberzon, I., Lim, M.M., McIntyre, C., Perrine, S.A., Risbrough, V.B., Sabban, E.L., Jeromin, A., Haas, M., 2021. Systematic review and methodological considerations for the use of single prolonged stress and fear extinction retention in rodents. Front. Behav. Neurosci. 15, 652636. https://doi.org/10.3389/fnbeh.2021.652636.

Friend, S.F., Nachnani, R., Powell, S.B., Risbrough, V.B., 2020. C-Reactive Protein: marker of risk for post-traumatic stress disorder and its potential for a mechanistic role in trauma response and recovery. Eur. J. Neurosci. https://doi.org/10.1111/ejn.15031.

Guo, B., Chen, J., Chen, Q., Ren, K., Feng, D., Mao, H., Yao, H., Yang, J., Liu, H., Liu, Y., Jia, F., Qi, C., Lynn-Jones, T., Hu, H., Fu, Z., Feng, G., Wang, W., Wu, S., 2019. Anterior cingulate cortex dysfunction underlies social deficits in Shank3 mutant mice. Nat. Neurosci. 22 (8), 1223–1234. https://doi.org/10.1038/s41593-019-0445-9.

Harnett, N.G., van Rooij, S.J.H., Ely, T.D., Lebois, L.A.M., Murty, V.P., Jovanovic, T., Hill, S.B., Dumornay, N.M., Merker, J.B., Bruce, S.E., House, S.L., Beaudoin, F.L., An, X., Zeng, D., Neylan, T.C., Clifford, G.D., Linnstaedt, S.D., Germine, L.T., Bollen, K.A., Rauch, S.L., Lewandowski, C., Hendry, P.L., Sheikh, S., Storrow, A.B., Musey Jr., P.I., Haran, J.P., Jones, C.W., Punches, B.E., Swor, R.A., McGrath, M.E., Pascual, J.L., Seamon, M.J., Mohiuddin, K., Chang, A.M., Pearson, C., Peak, D.A., Domeier, R.M., Rathlev, N.K., Sanchez, L.D., Pietrzak, R.H., Joormann, J., Barch, D.M., Pizzagalli, D.A., Sheridan, J.F., Harte, S.E., Elliott, J.M., Kessler, R.C., Koenen, K.C., McLean, S., Ressler, K.J., Stevens, J.S., 2021. Prognostic neuroimaging biomarkers of trauma-related psychopathology: resting-state fMRI shortly after trauma predicts future PTSD and depression symptoms in the AURORA study. Neuropsychopharmacology 46 (7), 1263–1271. https://doi.org/10.1038/s41386-020-00946-8.

Hartley, N.D., Gaulden, A.D., Baldi, R., Winters, N.D., Salimando, G.J., Rosas-Vidal, L.E., Jameson, A., Winder, D.G., Patel, S., 2019. Dynamic remodeling of a basolateral-to-central amygdala glutamatergic circuit across fear states. Nat. Neurosci. 22 (12), 2000–2012. https://doi.org/10.1038/s41593-019-0528-7.

Hartley, N.D., Gunduz-Cinar, O., Halladay, L., Bukalo, O., Holmes, A., Patel, S., 2016. 2-arachidonoylglycerol signaling impairs short-term fear extinction. Transl. Psychiatry 6, e749. https://doi.org/10.1038/tp.2016.26.

Hayes, J.P., Hayes, S.M., Mikedis, A.M., 2012. Quantitative meta-analysis of neural activity in posttraumatic stress disorder. Biol. Mood Anxiety Disord. 2, 9. https://doi.org/10.1186/2045-5380-2-9.

Hendricks, T.J., Fyodorov, D.V., Wegman, L.J., Lelutiu, N.B., Pehek, E.A., Yamamoto, B., Silver, J., Weeber, E.J., Sweatt, J.D., Deneris, E.S., 2003. Pet-1 ETS gene plays a critical role in 5-HT neuron development and is required for normal anxiety-like and aggressive behavior. Neuron 37 (2), 233–247. https://doi.org/10.1016/s0896-6273(02)01167-4.

Imanaka, A., Morinobu, S., Toki, S., Yamawaki, S., 2006. Importance of early environment in the development of post-traumatic stress disorder-like behaviors. Behav. Brain Res. 173 (1), 129–137. https://doi.org/10.1016/j.bbr.2006.06.012.

Imperatori, C., Farina, B., Quintiliani, M.I., Onofri, A., Castelli Gattinara, P., Lepore, M., Gnoni, V., Mazzucchi, E., Contardi, A., Della Marca, G., 2014. Aberrant EEG functional connectivity and EEG power spectra in resting state post-traumatic stress disorder: a sLORETA study. Biol. Psychol. 102, 10–17. https://doi.org/10.1016/j.biopsycho.2014.07.011.

Iwamoto, Y., Morinobu, S., Takahashi, T., Yamawaki, S., 2007. Single prolonged stress increases contextual freezing and the expression of glycine transporter 1 and vesicle-associated membrane protein 2 mRNA in the hippocampus of rats. Prog. Neuro-Psychopharmacol. Biol. Psychiatry 31 (3), 642–651. https://doi.org/10.1016/j.pnpbp.2006.12.010.

Johnson, E., McAlees, J., Lewkowich, I., Sah, R., 2021. Asthma and Posttraumatic Stress Disorder (PTSD): emerging links, potential models and mechanisms. Brain Behav. Immun. https://doi.org/10.1016/j.bbi.2021.06.001.

Kalin, N.H., 2021. Trauma, resilience, anxiety disorders, and PTSD. Am. J. Psychiatr. 178 (2), 103–105. https://doi.org/10.1176/appi.ajp.2020.20121738.

Kemp, A.H., Griffiths, K., Felmingham, K.L., Shankman, S.A., Drinkenburg, W., Arns, M., Clark, C.R., Bryant, R.A., 2010. Disorder specificity despite comorbidity: resting EEG alpha asymmetry in major depressive disorder and post-traumatic stress disorder. Biol. Psychol. 85 (2), 350–354. https://doi.org/10.1016/j.biopsycho.2010.08.001.

Khan, S., Liberzon, I., 2004. Topiramate attenuates exaggerated acoustic startle in an animal model of PTSD. Psychopharmacology (Berlin) 172 (2), 225–229. https://doi.org/10.1007/s00213-003-1634-4.

Kitayama, N., Vaccarino, V., Kutner, M., Weiss, P., Bremner, J.D., 2005. Magnetic resonance imaging (MRI) measurement of hippocampal volume in posttraumatic stress disorder: a meta-analysis. J. Affect. Disord. 88 (1), 79–86. https://doi.org/10.1016/j.jad.2005.05.014.

Koch, S.B., van Zuiden, M., Nawijn, L., Frijling, J.L., Veltman, D.J., Olff, M., 2016. Aberrant resting-state brain activity in posttraumatic stress disorder: a meta-analysis and systematic review. Depress. Anxiety 33 (7), 592–605. https://doi.org/10.1002/da.22478.

Liu, T., Bai, W., Wang, J., Tian, X., 2016. An aberrant link between gamma oscillation and functional connectivity in Abeta1-42-mediated memory deficits in rats. Behav. Brain Res. 297, 51–58. https://doi.org/10.1016/j.bbr.2015.10.008.

Lukas, M., Toth, I., Reber, S.O., Slattery, D.A., Veenema, A.H., Neumann, I.D., 2011. The neuropeptide oxytocin facilitates pro-social behavior and prevents social avoidance in rats and mice. Neuropsychopharmacology 36 (11), 2159–2168. https://doi.org/10.1038/npp.2011.95.

Milad, M.R., Pitman, R.K., Ellis, C.B., Gold, A.L., Shin, L.M., Lasko, N.B., Zeidan, M.A., Handwerger, K., Orr, S.P., Rauch, S.L., 2009. Neurobiological basis of failure to recall extinction memory in posttraumatic stress disorder. Biol. Psychiatr. 66 (12), 1075–1082. https://doi.org/10.1016/j.biopsych.2009.06.026.

Newson, J.J., Thiagarajan, T.C., 2018. EEG frequency bands in psychiatric disorders: a review of resting state studies. Front. Hum. Neurosci. 12, 521. https://doi.org/10.3389/fnhum.2018.00521.

Onslow, A.C., Bogacz, R., Jones, M.W., 2011. Quantifying phase-amplitude coupling in neuronal network oscillations. Prog. Biophys. Mol. Biol. 105 (1–2), 49–57. https://doi.org/10.1016/j.pbiomolbio.2010.09.007.

Orsillo, S.M., Heimberg, R.G., Juster, H.R., Garrett, J., 1996. Social phobia and PTSD in Vietnam veterans. J. Trauma Stress 9 (2), 235–252. https://doi.org/10.1007/BF02110658.

Paolini, A.G.A.G., 2014. <In vivo electrophysiological recordings in amygdala subnuclei reveal selective and distinct responses to a behaviorally identified predator odor>. J. Neurophysiol. https://doi.org/10.1152/jn.00373.2014.

Parks, C.L., Robinson, P.S., Sibille, E., Shenk, T., Toth, M., 1998. Increased anxiety of mice lacking the serotonin1A receptor. Proc. Natl. Acad. Sci. U. S. A. 95 (18), 10734–10739. https://doi.org/10.1073/pnas.95.18.10734.

Philippi, C.L., Velez, C.S., Wade, B.S.C., Drennon, A.M., Cooper, D.B., Kennedy, J.E., Bowles, A.O., Lewis, J.D., Reid, M.W., York, G.E., Newsome, M.R., Wilde, E.A., Tate, D.F., 2021. Distinct patterns of resting-state connectivity in U.S. service members with mild traumatic brain injury versus posttraumatic stress disorder. Brain Imag. Behav. https://doi.org/10.1007/s11682-021-00464-1.

Santiago, P.N., Ursano, R.J., Gray, C.L., Pynoos, R.S., Spiegel, D., Lewis-Fernandez, R., Friedman, M.J., Fullerton, C.S., 2013. A systematic review of PTSD prevalence and trajectories in DSM-5 defined trauma exposed populations: intentional and non-intentional traumatic events. PloS One 8 (4), e59236. https://doi.org/10.1371/journal.pone.0059236.

Schlenger, W.E., Caddell, J.M., Ebert, L., Jordan, B.K., Rourke, K.M., Wilson, D., Thalji, L., Dennis, J.M., Fairbank, J.A., Kulka, R.A., 2002. Psychological reactions to terrorist attacks: findings from the national study of Americans' reactions to september 11. J. Am. Med. Assoc. 288 (5), 581–588. https://doi.org/10.1001/jama.288.5.581.

Schlumpf, Y.R., Nijenhuis, E.R.S., Klein, C., Jancke, L., Bachmann, S., 2021. Resting-state functional connectivity in patients with a complex PTSD or complex dissociative disorder before and after inpatient trauma treatment. Brain Behav., e02200 https://doi.org/10.1002/brb3.2200.

Schutz, M., Oertel, B.G., Heimann, D., Doehring, A., Walter, C., Dimova, V., Geisslinger, G., Lotsch, J., 2014. Consequences of a human TRPA1 genetic variant on the perception of nociceptive and olfactory stimuli. PloS One 9 (4), e95592. https://doi.org/10.1371/journal.pone.0095592.

Shankman, S.A., Silverstein, S.M., Williams, L.M., Hopkinson, P.J., Kemp, A.H., Felmingham, K.L., Bryant, R.A., McFarlane, A., Clark, C.R., 2008. Resting electroencephalogram asymmetry and posttraumatic stress disorder. J. Trauma Stress 21 (2), 190–198. https://doi.org/10.1002/jts.20319.

Shin, L.M., Whalen, P.J., Pitman, R.K., Bush, G., Macklin, M.L., Lasko, N.B., Orr, S.P., McInerney, S.C., Rauch, S.L., 2001. An fMRI study of anterior cingulate function in posttraumatic stress disorder. Biol. Psychiatr. 50 (12), 932–942. https://doi.org/10.1016/s0006-3223(01)01215-x.

Shoji, H., Takao, K., Hattori, S., Miyakawa, T., 2014. Contextual and cued fear conditioning test using a video analyzing system in mice. JoVE 85. https://doi.org/10.3791/50871.

Stout, D.M., Glenn, D.E., Acheson, D.T., Simmons, A.N., Risbrough, V.B., 2019. Characterizing the neural circuitry associated with configural threat learning. Brain Res. 1719, 225–234. https://doi.org/10.1016/j.brainres.2019.06.003.

Taylor, J.E., Lau, H., Seymour, B., Nakae, A., Sumioka, H., Kawato, M., Koizumi, A., 2020. An evolutionarily threat-relevant odor strengthens human fear memory. Front. Neurosci. 14, 255. https://doi.org/10.3389/fnins.2020.00255.

Todder, D., Levine, J., Abujumah, A., Mater, M., Cohen, H., Kaplan, Z., 2012. The quantitative electroencephalogram and the low-resolution electrical tomographic analysis in posttraumatic stress disorder. Clin. EEG Neurosci. 43 (1), 48–53. https://doi.org/10.1177/1550059411428716.

Tursich, M., Neufeld, R.W., Frewen, P.A., Harricharan, S., Kibler, J.L., Rhind, S.G., Lanius, R.A., 2014. Association of trauma exposure with proinflammatory activity: a transdiagnostic meta-analysis. Transl. Psychiatry 4, e413. https://doi.org/10.1038/tp.2014.56.

Tynan, R.J., Naicker, S., Hinwood, M., Nalivaiko, E., Buller, K.M., Pow, D.V., Day, T.A., Walker, F.R., 2010. Chronic stress alters the density and morphology of microglia in a subset of stress-responsive brain regions. Brain Behav. Immun. 24 (7), 1058–1068. https://doi.org/10.1016/j.bbi.2010.02.001.

Wang, W., Liu, Y., Zheng, H., Wang, H.N., Jin, X., Chen, Y.C., Zheng, L.N., Luo, X.X., Tan, Q.R., 2008. A modified single-prolonged stress model for post-traumatic stress disorder. Neurosci. Lett. 441 (2), 237–241. https://doi.org/10.1016/j.neulet.2008.06.031.

Xia, L., Zhai, M., Wang, L., Miao, D., Zhu, X., Wang, W., 2013. FGF2 blocks PTSD symptoms via an astrocyte-based mechanism. Behav. Brain Res. 256, 472–480. https://doi.org/10.1016/j.bbr.2013.08.048.

Xu, H.Y., Liu, Y.J., Xu, M.Y., Zhang, Y.H., Zhang, J.X., Wu, Y.J., 2012. Inactivation of the bed nucleus of the stria terminalis suppresses the innate fear responses of rats induced by the odor of cat urine. Neuroscience 221, 21–27. https://doi.org/10.1016/j.neuroscience.2012.06.056.

Yabuki, Y., Fukunaga, K., 2019. Clinical therapeutic strategy and neuronal mechanism underlying post-traumatic stress disorder (PTSD). Int. J. Mol. Sci. 20 (15) https://doi.org/10.3390/ijms20153614.

Yamasue, H., Kasai, K., Iwanami, A., Ohtani, T., Yamada, H., Abe, O., Kuroki, N., Fukuda, R., Tochigi, M., Furukawa, S., Sadamatsu, M., Sasaki, T., Aoki, S., Ohtomo, K., Asukai, N., Kato, N., 2003. Voxel-based analysis of MRI reveals anterior cingulate gray-matter volume reduction in posttraumatic stress disorder due to terrorism. Proc. Natl. Acad. Sci. U. S. A. 100 (15), 9039–9043. https://doi.org/10.1073/pnas.1530467100.

Yehuda, R., 2002. Post-traumatic stress disorder. N. Engl. J. Med. 346 (2), 108–114. https://doi.org/10.1056/NEJMra012941.

Zhou, T., Zhu, H., Fan, Z., Wang, F., Chen, Y., Liang, H., Yang, Z., Zhang, L., Lin, L., Zhan, Y., Wang, Z., Hu, H., 2017. History of winning remodels thalamo-PFC circuit to reinforce social dominance. Science 357 (6347), 162–168. https://doi.org/10.1126/science.aak9726.

Zhou, Y.G., Shang, Z.L., Zhang, F., Wu, L.L., Sun, L.N., Jia, Y.P., Yu, H.B., Liu, W.Z., 2021. PTSD: past, present and future implications for China. Chin. J. Traumatol. https://doi.org/10.1016/j.cjtee.2021.04.011.

Zhou, Z., Liu, X., Chen, S., Zhang, Z., Liu, Y., Montardy, Q., Tang, Y., Wei, P., Liu, N., Li, L., Song, R., Lai, J., He, X., Chen, C., Bi, G., Feng, G., Xu, F., Wang, L., 2019. A VTA GABAergic neural circuit mediates visually evoked innate defensive responses. Neuron 103 (3), 473–488. https://doi.org/10.1016/j.neuron.2019.05.027 e476.

Zoladz, P.R., Fleshner, M., Diamond, D.M., 2012. Psychosocial animal model of PTSD produces a long-lasting traumatic memory, an increase in general anxiety and PTSD-like glucocorticoid abnormalities. Psychoneuroendocrinology 37 (9), 1531–1545. https://doi.org/10.1016/j.psyneuen.2012.02.007.

Zweerings, J., Pflieger, E.M., Mathiak, K.A., Zvyagintsev, M., Kacela, A., Flatten, G., Mathiak, K., 2018. Impaired voluntary control in PTSD: probing self-regulation of the ACC with real-time fMRI. Front. Psychiatr. 9, 219. https://doi.org/10.3389/fpsyt.2018.00219.